Thin Solid Films 582 (2015) 300–303

Contents lists available at ScienceDirect

Thin Solid Films

journal homepage: www.elsevier.com/locate/tsf

Highly reflective rear surface passivation design for ultra-thin Cu(In,Ga)Se_2 solar cells

Bart Vermang [a,b,*], Jörn Timo Wätjen [a], Viktor Fjällström [a], Fredrik Rostvall [a], Marika Edoff [a], Rickard Gunnarsson [c], Iris Pilch [c], Ulf Helmersson [c], Ratan Kotipalli [d], Frederic Henry [d], Denis Flandre [d]

[a] Ångström Solar Center, University of Uppsala, Uppsala 75121, Sweden
[b] ESAT-KU Leuven, University of Leuven, Leuven 3001, Belgium
[c] Plasma & Coatings Physics, University of Linköping, Linköping 58183, Sweden
[d] ICTEAM/IMNC, Université Catholique de Louvain, Louvain-la-Neuve 1348, Belgium

ARTICLE INFO

Available online 30 October 2014

Keywords:
Ultra-thin films
Copper Indium Gallium Selenide
Aluminum oxide
Surface passivation layer
Molybdenum
Nanoparticles
Local contacts
Solar cells

ABSTRACT

Al_2O_3 rear surface passivated ultra-thin Cu(In,Ga)Se_2 (CIGS) solar cells with Mo nano-particles (NPs) as local rear contacts are developed to demonstrate their potential to improve optical confinement in ultra-thin CIGS solar cells. The CIGS absorber layer is 380 nm thick and the Mo NPs are deposited uniformly by an up-scalable technique and have typical diameters of 150 to 200 nm. The Al_2O_3 layer passivates the CIGS rear surface between the Mo NPs, while the rear CIGS interface in contact with the Mo NP is passivated by [Ga]/([Ga] + [In]) (GGI) grading. It is shown that photon scattering due to the Mo NP contributes to an absolute increase in short circuit current density of 3.4 mA/cm^2; as compared to equivalent CIGS solar cells with a standard back contact.

1. Introduction

One way to lower the cost of Cu(In,Ga)Se_2 (CIGS) solar cells is to reduce the thickness of the CIGS absorber layer (t_{CIGS}). First, this approach will cut material usage – critical feedstock materials are In and Ga [1] – and thus material cost. Furthermore, t_{CIGS} reduction has the potential to increase manufacturing output due to shortened deposition times. And, finally, using less absorber material might even lead to higher efficiencies thanks to the associated reduction in bulk defects (i.e. if optical confinement and rear surface passivation are kept satisfactory).

However, reducing t_{CIGS} below 500 nm in standard CIGS solar cells decreases cell efficiency considerably because of high recombination and low reflection at a regular Mo/CIGS rear interface [2–4]. A loss in efficiency that is caused by a decrease in both open circuit voltage (V_{OC}) and short circuit current density (J_{SC}); see Fig. 1(a) and (b), respectively. The loss in V_{OC} is due to the highly recombinative Mo/CIGS rear interface (the rear surface recombination velocity (S_b) is between 1×10^4 and 1×10^6 cm/s) that becomes a more effective recombination-plane with reduced CIGS thickness. The loss in J_{SC} is due to the poorly reflective Mo/CIGS rear interface (the rear internal reflection (R_b) is below 60%) causing incomplete absorption in the absorber layer.

Recombination at the Mo/CIGS rear interface can be reduced by introduction of a rear surface passivation layer with nano-sized point openings [3,4]. This idea stems from the Si solar cell industry, where rear surface passivation layers are combined with micron-sized point openings to boost V_{OC}, see e.g. Ref. [5]. The passivation layer is known to reduce interface recombination by chemical (equals a reduction in interface trap density at the rear CIGS surface) and field-effect passivation (equals a fixed charge density in the passivation layer that reduces the surface minority or majority charge carrier concentration), while the point openings allow for contacting. Such a typical Si surface passivation layer is Al_2O_3, as described in Ref. [6]. In Refs. [3,4,7], equivalent Al_2O_3 layers are used to passivate the rear CIGS surface and the formation of nano-sphere shaped precipitates in chemical bath deposition (CBD) of CdS to generate point contact openings. This way, an obvious increase in V_{OC} is measured for the rear passivated CIGS solar cells with ultra-thin absorber layers compared to corresponding unpassivated standard cells, as is shown in Fig. 1(a). Moreover, using a solar cell capacitance simulator (SCAPS) to model the Al_2O_3 rear surface passivated cells, the minimal S_b has been estimated to be as low as 100 cm/s [3]. Note that comparing the V_{OC} of rear surface passivated Si solar cells and unpassivated reference cells (see e.g. Fig. 4 in [5]) shows a very similar tendency as depicted in Fig. 1(a).

Additionally, also rear reflection can be enhanced by applying the same advanced rear contacting structure [7]. In Si solar cells, R_b is optimized applying rear surface passivation layer stacks with a total

* Corresponding author at: Ångström Solar Center, University of Uppsala, Uppsala 75121, Sweden. Tel.: +46 18 471 7238; fax: +46 18 55 50 95.
E-mail address: Bart.Vermang@angstrom.uu.se (B. Vermang).

http://dx.doi.org/10.1016/j.tsf.2014.10.050

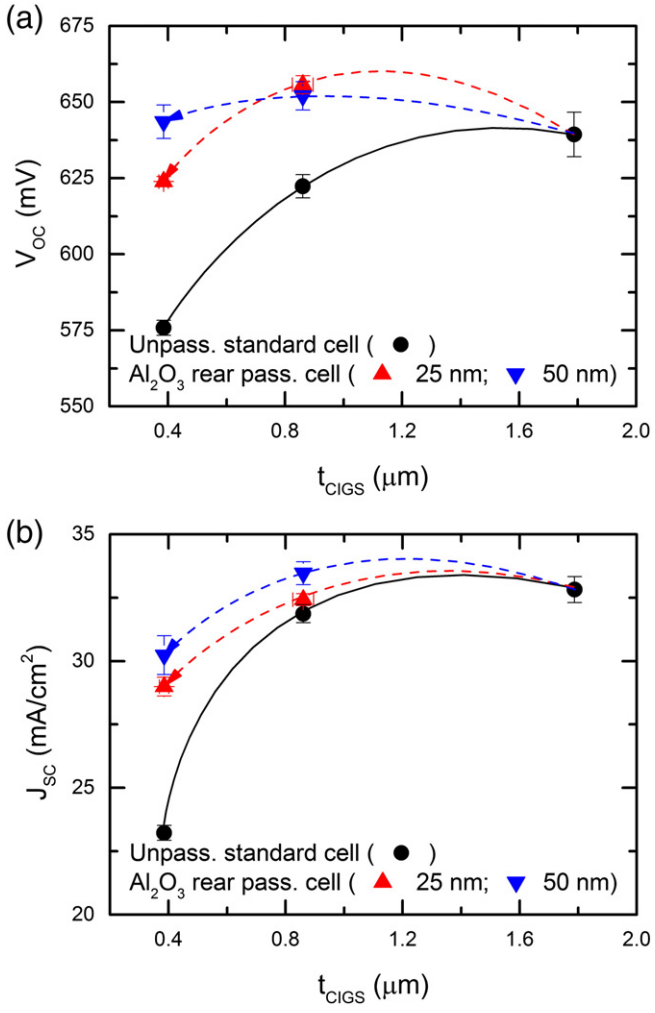

Fig. 1. Average (a) open circuit voltage and (b) short circuit current density as a function of CIGS absorber layer thickness for Al_2O_3 rear surface passivated CIGS solar cells having nano-sized local rear point contacts compared to unpassivated standard cells. For all cells, GGI is constant and equals 30%. Standard deviation is shown as error bars and lines serve as a guide to the eye.

thickness of several hundreds of nanometers [8]. Equally, in Ref. [7] rear internal reflection is improved by increasing the thickness of the Al_2O_3 passivation layer, or stacking a thin Al_2O_3 interface passivation layer on top of another thick layer (e.g. MgF_2). Hence, J_{SC} is enhanced substantially for the ultra-thin rear passivated solar cells compared to matching unpassivated standard reference cells, as shown in Fig. 1(b). Note that there is a practical limit to increasing the thickness of the rear surface passivation layer as the CIGS absorber layer itself is only a few hundreds of nanometers thick.

Due to reflection limitations of passivation layers, supplementary ways to optimize optical confinement in ultra-thin CIGS solar cells are needed. In Fig. 1(b), there is still a difference in J_{SC} between rear passivated ultra-thin CIGS cells and standard thick cells, while J_{SC} losses can be completely avoided for rear passivated Si solar cells with reduced Si thickness (see e.g. Fig. 3 in [8]). As this loss in J_{SC} is mainly caused by rear reflected photons escaping at the front surface of the solar cell, additional methods to prolong the travel path of photons are sought for.

In this work, rear surface passivated CIGS solar cells with Mo nanoparticles (NPs) as local rear contacts are developed to demonstrate that these Mo NPs show potential to improve optical confinement of ultra-thin CIGS solar cells by increased scattering of photons.

2. Experimental details

The Mo NPs are deposited uniformly by an upscalable technique and have typical diameters of about 150 to 200 nm. Negatively charged Mo NPs are first grown in a highly ionized pulsed plasma and then – thanks to their electrostatic repulsion – evenly spread onto a Mo coated soda lime glass (SLG) substrate; as described in more depth in Refs. [9,10]. A top-view scanning electron microscopy picture of Mo NP on a SLG/Mo substrate is shown in Fig. 2. This Mo NP density has been chosen, as it is comparable to the density of the CdS NP in Refs. [3,4,7] (used to create point contact openings in Al_2O_3 rear passivated CIGS solar cells).

A summary of the applied cell processing steps is given in Table 1; a more detailed description of the fabricated 0.5 cm^2 SLG/Mo(/Mo NP/Al_2O_3)/CIGS/CdS/i-ZnO/ZnO:Al(/MgF_2 anti-reflective coating (ARC)) solar cell devices with thin co-evaporated CIGS absorber layers, and the performed J–V and external quantum efficiency (EQE) measurements can be found elsewhere [3,4,7].

A cross section picture of an Al_2O_3 rear surface passivated CIGS solar cell with Mo NP contacts can be found in Fig. 3: (a) A transmission electron microscopy (TEM) cross section picture and (b) an energy-dispersive X-ray spectroscopy (EDS) map for the elements Cu, Al and Mo in such a cross section.

3. Results and discussion

3.1. Constant GGI

Introducing Mo NP at the Mo/CIGS rear interface increases photon scattering, but also recombination, which can be partly off-set by passivating the Mo/CIGS interface between the NPs with Al_2O_3. Table 2 gives an overview of average cell characterization results of unpassivated CIGS solar cells with and without Mo NP at the Mo/CIGS interface as well as Al_2O_3 rear surface passivated CIGS solar cells with Mo NP contacts. In all cases, the t_{CIGS} is 350 nm with the [Ga]/([Ga] + [In]) (GGI) ratio constant and equal to 30%. This table shows that introducing Mo NP at the rear interface of standard CIGS solar cells lowers V_{OC} and increases J_{SC}. This lower V_{OC} and higher J_{SC} can be explained by respectively the increase in Mo/CIGS interface area and the increase in photon scattering, both due to the Mo NP. However, direct current (DC) sputtering of a thin Al_2O_3 layer (10–15 nm, see Fig. 3(b)) on the 150–200 nm Mo NP before CIGS deposition passivates the Mo/CIGS interface between the NPs and reduces this loss in V_{OC}. Also, the reasonable fill factor (FF) of these Al_2O_3 rear passivated cells shows that – thanks to the characteristic directionality of sputtering processes – parts of the Mo NP remain uncovered and thus serve as rear contacting area, as

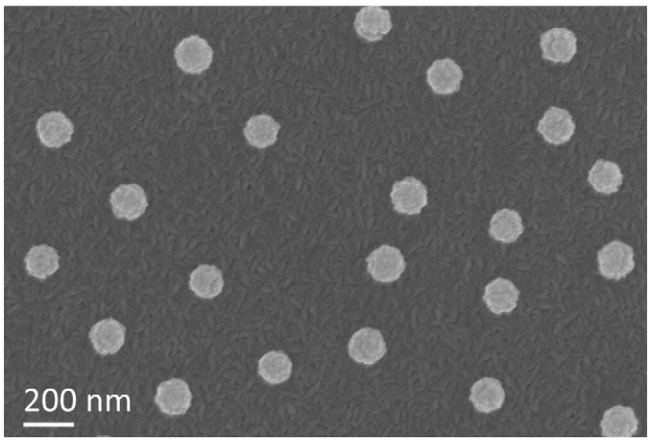

Fig. 2. Top-view scanning electron microscopy picture of the Mo nano-particles deposited on a SLG/Mo substrate.

Table 1
Overview of all steps required to fabricate Al_2O_3 rear surface passivated CIGS solar cells with Mo NP contacts. Note that unpassivated standard cells are fabricated using the same processing sequence, but without steps 3 and 4.

Step	Description
0	Start = soda lime glass
1	Glass cleaning
2	Mo rear contact sputtering
3	Mo NP contact deposition
4	Thin Al_2O_3 passivation layer; DC-sputtering
5	NaF evaporation
6	Ultra-thin CIGS absorber co-evaporation
7	CBD CdS buffer deposition
8	(i-)ZnO(:Al) window sputtering
9	Ni/Al/Ni front contact evaporation
10	0.5 cm^2 solar cell scribing
11	MgF_2 ARC evaporation

already seen in Fig. 3(b). However, there is a residual loss (relative loss = 11%) in V_{OC} compared to the unpassivated standard cells without Mo NP, since the total unpassivated surface area of the Mo NP still remains large. A few notes: (i) a simple estimation indicates that the Mo/CIGS contacting area in the standard unpassivated cells and passivated cells with Mo NP is in the same order, if one takes into account that the particles are not completely spherical and that there is uncoated Mo/CIGS area around the Mo NP after Al_2O_3 sputtering (see Figs. 2 and 3); and (ii) The Mo NPs modify both the rear Mo/CIGS and front CIGS/CdS interfaces (see e.g. the "bumps" at the front surface of the CIGS layer just above the Mo nanoparticles in Fig. 3(a)). Hence, it is indeed more accurate to say that both scattering due to the increased roughness of front and rear CIGS surfaces will contribute to the J_{SC} improvement, as measured for solar cells with Mo NP. However, a more detailed front scattering and back reflection study is needed to separate both contributions.

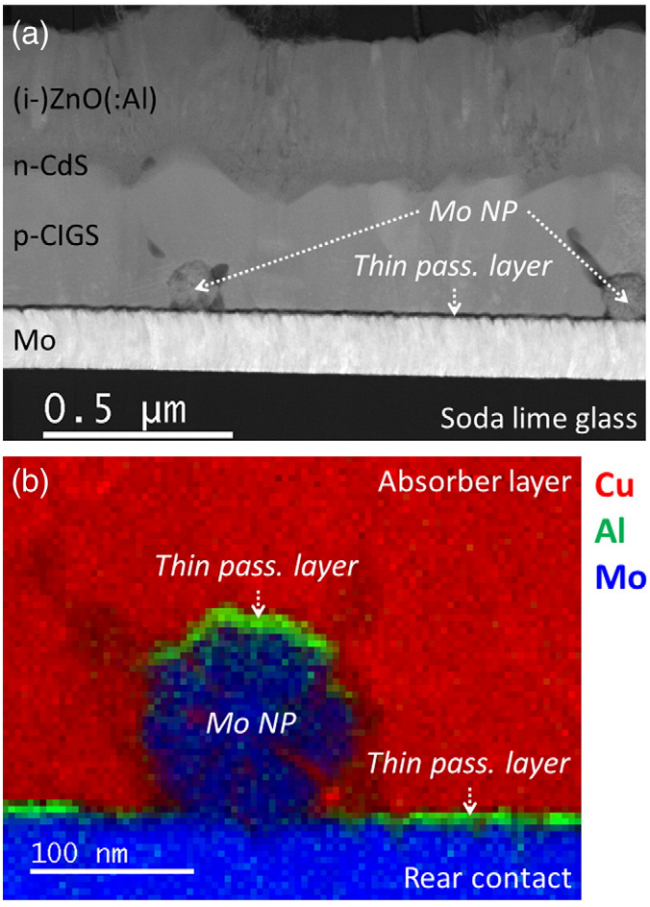

Fig. 3. (a) Transmission electron microscopy cross-section picture of an Al_2O_3 rear surface passivated CIGS solar cell with Mo NP contacts, and (b) an energy-dispersive X-ray spectroscopy map for the elements Cu, Al and Mo in such a cross-section.

Table 2
Overview of average cell characterization results (AM1.5 G) for 0.5 cm^2 unpassivated standard CIGS solar cells (with and without Mo NP at the Mo/CIGS interface) and Al_2O_3 rear surface passivated cells with Mo NP contacts. GGI is constant and equals 30%; and t_{CIGS} is 350 nm. Note that these cells are without an anti-reflective coating.

Cell description (no ARC)	# cells	V_{OC} (mV)	J_{SC} (mA/cm^2)	FF (%)	Eff. (%)
Standard	6	572 ± 07	20.4 ± 0.6	70 ± 2	8.2 ± 0.4
Standard + Mo NP	6	347 ± 10	21.7 ± 0.3	43 ± 3	3.2 ± 0.3
Standard + Mo NP + Al_2O_3	6	508 ± 39	22.1 ± 0.4	57 ± 3	6.4 ± 0.9

3.2. Single-graded GGI

Introducing a back surface field (BSF) in the CIGS absorber layer to passivate the Mo NP surface area in contact with this absorber layer lowers recombination even further. Table 2 gives an overview of standard cells with and without Mo NP and rear passivated cells with Mo NP contacts, but now GGI is single-graded (from 40% (rear) down to 20% (front)) and t_{CIGS} equals 380 nm. Such a GGI gradient is known to create a BSF, which will reduce recombination in the rear part of the cell. However, this strategy also leads to another absorption profile in spite of the similar average GGI ratio as compared with the cells presented in Section 3.1. Also in the case of single-graded GGI, standard cells with Mo NP lose V_{OC} and gain J_{SC} compared to standard cells without Mo NP, and this loss in V_{OC} is reduced by implementing an Al_2O_3 rear surface passivation layer. This time a relative loss in average V_{OC} of 7% remains between rear passivated cells with Mo NP and standard cells (which is lower than when a uniform GGI is used, because of the BSF). Comparing the rear passivated cells with Mo NP to the standard cells in more detail, there is a small increase in average efficiency (0.4% absolute) thanks to a clear increase in J_{SC} (3.4 mA/cm^2 absolute) but correlated to a decrease in V_{OC}. Representative J–V and EQE curves of all these cells can be found in Fig. 4. The J–V graph shows that the FF is low for the standard cells with Mo NP, due to an increase in series resistance (R_s) and shunt conductance (G_{sh}) compared with standard cells without Mo NP. G_{sh} is increased due to an increase in rear surface recombination (more recombination current due to the large Mo/CIGS interface area); while R_s is increased as the contact grid of Mo NP is only sub-optimized (the Mo NP process is highly randomized). For the rear passivated cells with Mo NP, G_{sh} is at the same level as the standard cells without Mo NP (as the rear surface passivation is at the same level), and R_s is still higher compared with these standard cells (also here, the contact grid of Mo NP is only sub-optimized). The EQE curves show increased photon absorption in a broad wavelength range for the (rear passivated) cells with Mo NP. Additionally, Fig. 4(b) also shows that this increase in EQE is mainly caused by increased photon scattering due to the Mo NP (as expected, since passivation layer reflection is negligible for such a thin Al_2O_3 layer [4]). However, a more detailed optical confinement study is needed to quantify the Mo NP scattering and passivation layer reflection contributions.

Table 3
Overview of average cell characterization results (AM1.5 G) for 0.5 cm^2 unpassivated standard CIGS solar cells (with and without Mo NP) and Al_2O_3 rear surface passivated cells with Mo NP contacts. GGI is single-graded: from 40% (rear) down to 20% (front); and t_{CIGS} is 380 nm.

Cell description	# cells	V_{OC} (mV)	J_{SC} (mA/cm^2)	FF (%)	Eff. (%)
Standard	6	568 ± 17	22.2 ± 0.4	67 ± 7	8.4 ± 1.3
Standard + Mo NP	6	463 ± 20	25.3 ± 0.5	49 ± 3	5.8 ± 0.7
Standard + Mo NP + Al_2O_3	6	530 ± 31	25.7 ± 0.4	65 ± 2	8.8 ± 0.8

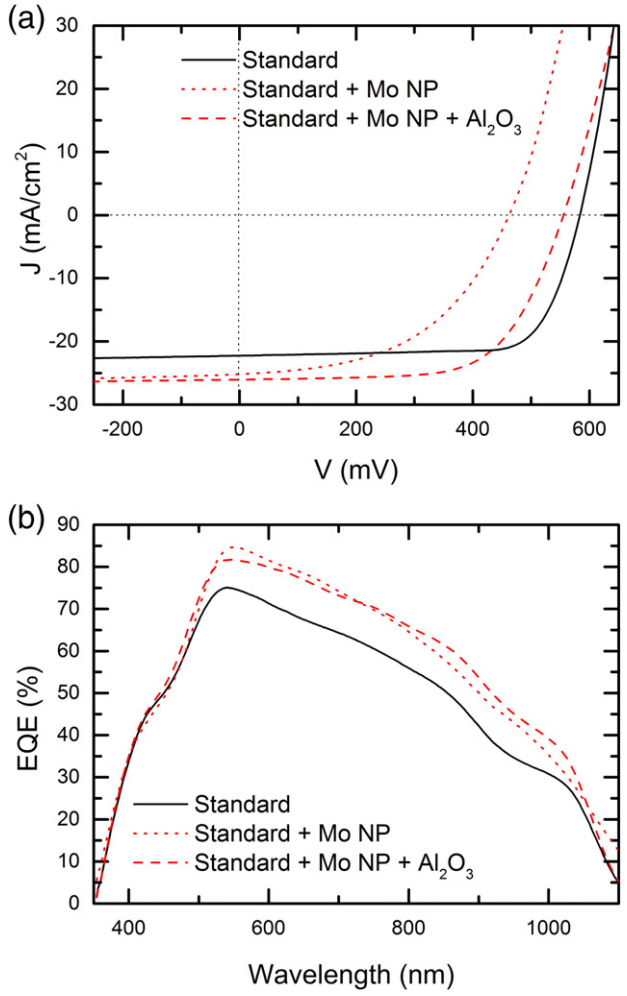

Fig. 4. Representative (a) J–V and (b) EQE curves for Al_2O_3 rear surface passivated CIGS solar cells with Mo NP contacts and corresponding unpassivated standard cells (with and without Mo NP). GGI is single-graded: from 40% (rear) down to 20% (front); and t_{CIGS} is 380 nm. See also Table 3.

4. Conclusions and outlook

Mo NP can potentially optimize light management in ultra-thin CIGS solar cells, if recombination at the large Mo/CIGS interface area is kept sufficiently low. Proof-of-principle ultra-thin ($t_{CIGS} = 380$ nm) Al_2O_3 rear surface passivated CIGS solar cells with Mo NPs as local rear contacts have been developed with an average efficiency of 8.8%. The Al_2O_3 layer passivates the CIGS rear surface between the Mo NPs, while the impact of the highly recombinative rear CIGS interface in contact with the Mo NP is reduced by GGI grading. It is shown that photon scattering due to the increased roughness of front and rear CIGS surfaces contributes to a clear increase in J_{SC}, as compared to corresponding ultra-thin standard CIGS solar cells.

There is still room to improve the suggested approach through e.g. (i) fine-tuning the shape, size and density of the Mo NP (to optimize scattering or obtain plasmonic light trapping), (ii) improvement of the passivation layer quality (thickness, alternative layers), (iii) reduction of the series resistance of the cells (adapted cell processing), and (iv) refinement of the GGI profile (double-grading).

Acknowledgments

This work is funded by the European Commission via FP7 Marie Curie IEF 2011 Action No. 300998, the Knut and Alice Wallenberg Foundation through Grant No. 2012.0083 and the Swedish Research Council under Grant No. 2008-6572 via the Linköping Linnaeus Environment LiLi-NFM. Lastly, F.H. would like to thank the European and Wallonia Region FEDER Grant ECP12020011678F (MINATIS project) for the financial support.

References

[1] M. Woodhouse, A. Goodrich, R. Margolis, T.L. James, M. Lokanc, R. Eggert, Supply-chain dynamics of tellurium, indium, and gallium within the context of PV manufacturing costs, IEEE J. Photovolt. 3 (2013) 833.
[2] W.N. Shafarman, R.S. Huang, S.H. Stephens, Characterization of Cu(InGa)Se_2 solar cells using etched absorber layers, Proc. 4th World Conf. on Photovoltaic Energy Conversion, Waikoloa, Hawaii, USA, May 2006, IEEE, New York, 2006, p. 420.
[3] B. Vermang, V. Fjällström, J. Pettersson, P. Salomé, M. Edoff, Development of rear surface passivated Cu(In, Ga)Se_2 thin film solar cells with nano-sized local rear point contacts, Sol. Energy Mater. Sol. Cells 117 (2013) 505.
[4] B. Vermang, V. Fjällström, X. Gao, M. Edoff, Improved rear surface passivation of Cu(In, Ga)Se_2 solar cells: a combination of an Al_2O_3 rear surface passivation layer and nanosized local rear point contacts, IEEE J. Photovolt. 4 (2014) 486.
[5] G. Agostinelli, P. Choulat, H.F.W. Dekkers, E. Vermariën, G. Beaucarne, Rear surface passivation for industrial solar cells on thin substrates, Proc. 4th World Conf. on Photovoltaic Energy Conversion, Waikoloa, Hawaii, USA, May 2006, IEEE, New York, 2006, p. 1004.
[6] G. Dingemans, W.M.M. Kessels, Status and prospects of Al_2O_3-based surface passivation schemes for silicon solar cells, J. Vac. Sci. Technol. A 30 (2012) 040802.
[7] B. Vermang, J.T. Wätjen, V. Fjällström, F. Rostvall, M. Edoff, R. Kotipalli, F. Henry, D. Flandre, Employing Si solar cell technology to increase efficiency of ultra-thin Cu(In, Ga)Se_2 solar cells, Prog. Photovolt. Res. Appl. 22 (10) (2014) 1023.
[8] G. Agostinelli, P. Choulat, H.F.W. Dekkers, Y. Ma, G. Beaucarne, Silicon solar cells on ultra-thin substrates for large scale production, Proc. 21st European Photovoltaic Solar Energy Conf., Dresden, Germany, September 2006, WIP, Munich, 2006, p. 601.
[9] I. Pilch, D. Söderström, N. Brenning, U. Helmersson, Size-controlled growth of nanoparticles in a highly ionized pulsed plasma, Appl. Phys. Lett. 102 (2013) 033108.
[10] I. Pilch, D. Söderström, D. Lundin, U. Helmersson, The use of highly ionized pulsed plasmas for the synthesis of advanced thin films and nanoparticles, KONA Powder Part. J. 31 (2014) 171.